Desalination and Water Treatment
www.deswater.com

21 (2010) 162–174
September

1944-3994/1944-3986
doi: 10.5004/dwt.2010.1325

Novel polymer film heat exchangers for seawater desalination

Jochen B.P. Christmann, Lorenz J. Krätz, Hans-Jörg Bart*

Lehrstuhl für Thermische Verfahrenstechnik, TU Kaiserslautern, P.O. Box: 3049, 67653 Kaiserslautern, Germany
Tel. +496312052414; Fax: +496312052119; email: bart@mv.uni-kl.de

Received 30 April 2009; accepted 14 March 2010

ABSTRACT

Multi-effect distillation (MED) plants with co-current flow show moderate process conditions with respect to temperature and pressure differences between consecutive effects. Thus, polymers seem to be best suited as a low-cost and less-corrodible alternative to metal alloys. Furthermore, polymer surfaces are less susceptible to scaling. In order to proof this concept, a falling film plate evaporator with heat transfer surfaces made of polyetheretherketone (PEEK) films was built. One of the main challenges is to assure a sufficient mechanical stability of the polymer film and simultaneously provide a low thermal resistance for heat conduction. Calculations and experiments show that a polymer film thickness of 25 μm, in combination with an appropriate spacer geometry, is sufficient for mechanical stability in MED plants. This low film thickness results in a thermal resistance for heat conduction comparable to 1.5 mm thick stainless steel. In order to demonstrate the applicability of polymer films for heat transfer surfaces, experimental investigations of the overall heat transfer coefficient were carried out at different operating conditions with a pilot plant scale polymer film heat exchanger.

Keywords: PEEK; Polymer film; Mechanical stability; Heat exchanger; Heat transfer; Falling film; Evaporation

1. Introduction

The implications of high material costs for metals have had dramatic impact on delivery periods and costs for metallic heat exchangers and evaporators. Though there was a cut in prices, metals are a limited resource and prices will increase most likely on a long-term view. For this reason, the substitution of metals and metal alloys by polymers may be a reasonable alternative to cut high material costs [1]. Heat exchangers consisting of different polymeric materials can be used in a wide range of applications [2] and they are already commercial available. They offer several advantages in comparison to metallic heat exchangers, such as corrosion resistance and weight reduction [1–4].

*Corresponding author

1.1. Heat transfer

One drawback of most polymers is their low thermal conductivity of about 0.1–0.5 W/(m·K) [1,5]. But the thermal conductivity has to be considered in conjunction with the convective heat transfer coefficients on both sides of the heat transfer surface. The basic equation for the calculation of the overall heat transfer coefficient through a plane wall without fouling consists of two convection terms (h_c, h_h) and one conduction term (k_{wall}):

$$\frac{1}{U \cdot A} = \frac{1}{h_c \cdot A} + \frac{L}{k_{wall} \cdot A} + \frac{1}{h_h \cdot A}. \quad (1)$$

In applications with condensation on one side and evaporation on the other side of the heat transfer surface,

Table 1
Comparison of mechanical and thermal properties for polypropylene homopolymer (PP-H), 25 μm thick polyetheretherketone film (PEEK 25 μm) and stainless steel (1.4571) at ambient temperature (20–25 °C) [5,7,9,10]

	PP-H	PEEK 25 μm	1.4571
Maximum allowed tensile stress $\sigma_{allowed}$ [MPa]	30	130	500 to 700
Young's modulus E [MPa]	1400	3000	200000
Thermal conductivity k [W/(m·K)]	0.22	0.25	15.0
Linear coefficient of thermal expansion α [K^{-1}]	100×10^{-6}	47×10^{-6}	16.5×10^{-6}

the convective heat transfer coefficients are usually high. Here, the overall heat transfer coefficient is strongly dependent on the thermal resistance of conduction. Polymeric heat transfer surfaces used for these applications must have a thermal resistance of conduction comparable to metallic heat exchangers to be competitive. 1 m^2 of 1.5 mm stainless steel (1.4571), for instance, has a thermal resistance of conduction of 1×10^{-4} K/W. The low thermal conductivity of polymers can be counteracted by the use of a very small wall thickness. A polymer film made of polyetheretherketone (PEEK) with wall thickness of 25 μm exhibits the same thermal resistance as 1.5 mm stainless steel (1.4571), if the same heat transfer area is assumed. These thin polymer films in turn, lead to a low mechanical strength of the heat transfer surface. The polymer film must be stabilised by spacers to withstand the pressure difference between the two sides of the heat transfer surface.

Co-current multi effect distillation (MED) is a process where the temperatures and the pressure differences applied, are moderate compared to most other distillation processes. Top brine temperatures (TBT) and pressure differences usually do not exceed 70°C [6] and 6,000 Pa, respectively, in low temperature MED plants. Because of those small thermal and mechanical loads, MED seems to be best suited for polymer film heat exchangers. In order to prove the applicability of polymeric heat transfer surfaces in MED, mechanical and thermal investigations were carried out. A pilot falling film plate heat exchanger was developed to show the feasibility of this concept.

1.2. Material selection

In order to reduce the thermal resistance of heat conduction, PEEK films (APTIV™ 1000, Victrex plc.) with a thickness of 25 μm were used as heat transfer surfaces. PEEK (polyetheretherketone) is a high performance polymer with excellent mechanical properties and a high continuous operating temperature (Table 1). Furthermore it meets the demands of FDA 21 CFR 177.2415 [7]. PEEK was already used in investigations on polymer film heat exchangers [8].

2. PEEK film elongation measurements

2.1. Experimental set-up

The mechanical properties of different polymers can be found in literature [5,9]. Unfortunately, the standardised test conditions for the determination of polymer properties, usually do not cover the process conditions in desalination plants. In order to meet our needs, a test-rig (Fig. 1) was built to investigate the creeping behaviour of the PEEK film under more realistic conditions with respect to temperature and the influence of water. The test-rig was placed into a temperature controlled water bath, filled with distilled water at 30 and 72°C, respectively. The width of the test strips was chosen with respect to the expected mechanical load during operation. Therefore the 25 μm thick polymer film was cut into small test stripes of a defined width (4.5 mm). The stripes had a length of 450 mm and they were marked at two points at a distance of 250 mm for elongation measurements. To exclude an influence of swelling by water uptake and thermal expansion to the elongation measurements, the stripes were stored at test conditions without mechanical stress for at least one day before starting the experiments. The stripes were then clamped into the test rig on one end. The other end of the polymer stripe was guided over a deviated roller and fixed to a particular weight. This leads to a certain tensile stress within the polymer film stripe during the entire test duration. The buoyancy force of the weight was taken into account and the distance between the two marked points was

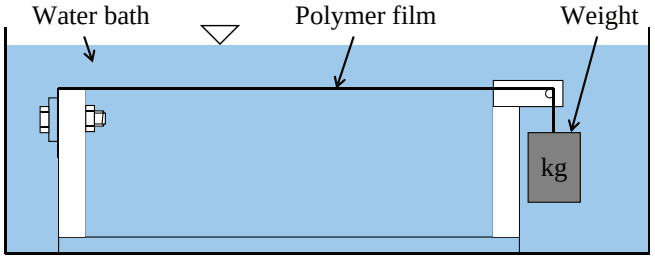

Fig. 1. Test-rig for mechanical experiments.

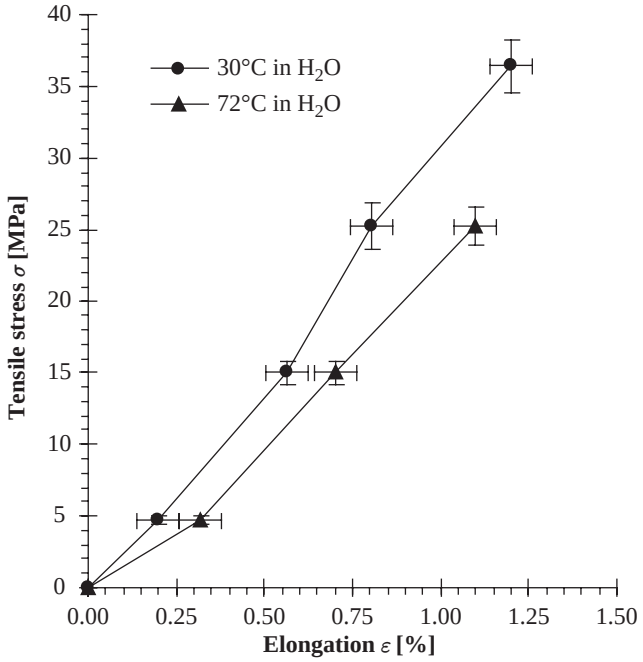

Fig. 2. Short-term stress-strain diagram for 25 μm thick PEEK film in distilled water.

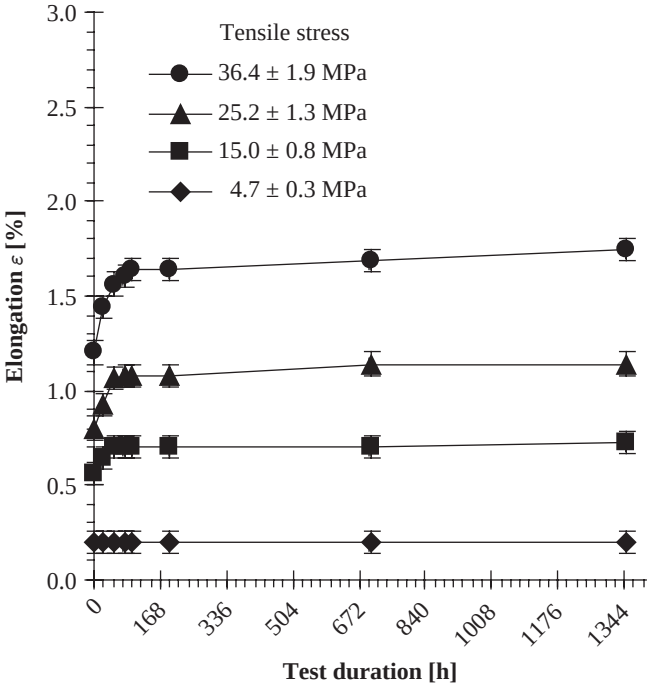

Fig. 3. PEEK film elongation at 30°C in distilled water.

measured with a sliding caliper to determine the elongation.

2.2. Elongation measurement results

Polymers exhibit visco-elastic properties [5]. Depending on the polymer, the elongation is increasing and the Young's modulus is decreasing with time when a constant load is applied. Hence, Young's modulus E has to be replaced by the creeping modulus E_{Cr} when creeping occurs. Only the short-term elongation can still be described by the Young's modulus. The short term stress-strain diagram of 25 μm thick PEEK film in distilled water at two different temperatures is shown in Fig. 2. It was observed that the elongation increases with temperature at a given tensile stress. Consequently, the mean value of the Young's modulus (short-term creeping modulus) is decreasing with temperature (Table 2).

The experimental results in Fig. 2 provide information about the short-term mechanical behaviour of PEEK films under mechanical stress in water. The vendor reports a Young's modulus of 3000 MPa for 25 μm thick PEEK film according to ISO 527 at 23°C [7]. Considering the different temperatures, it can be concluded, that the observed mean value of about 2800 MPa for the Young's modulus at 30°C in water is in good agreement with the vendor's information, although the experimental setup is not compliant with ISO 527.

Table 2
Mean Young's modulus of 25 μm thick PEEK film in distilled water (elongation < 1.50%)

Temperature ϑ [°C]	30	72
Mean Young's modulus E [MPa]	2796 ± 156	1970 ± 79

The elongation was also measured in distilled water over an extended period of time in order to investigate the creeping behaviour of the 25 μm thick PEEK film (Figs. 3 and 4). It can be seen, that the temperature has significant influence on mechanical properties, especially at higher tensile stress. Mechanical breakdown of the polymer film was observed at a tensile stress of 45.4 MPa and 72°C after less than 1152 h (data not shown). The vendor specifies an allowed tensile stress for PEEK film (50 μm) of approximately 60 MPa at 200°C according to ISO 527 [7]. It is necessary to remember, that the experimental conditions were selected with focus on the operating conditions of a MED plant and therefore were not in compliance with ISO 527. Furthermore, the tensile stress applied to the polymer film is always referred to the primarily film cross-sectional area. Elongation of the polymer film leads to a decrease of the cross-sectional area and consequently to an increase of the effective tensile stress. If the tensile stress is too high and creeping elongation is continuing without stopping, this will inevitably cause

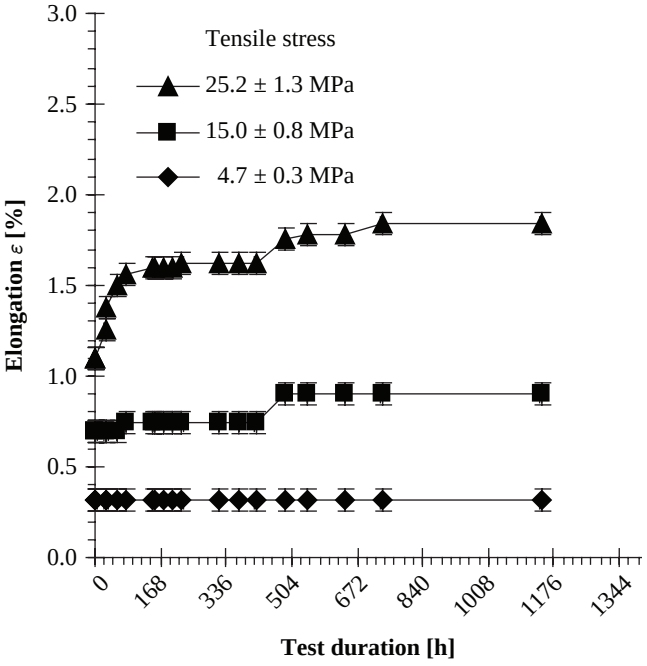

Fig. 4. PEEK film elongation at 72°C in distilled water.

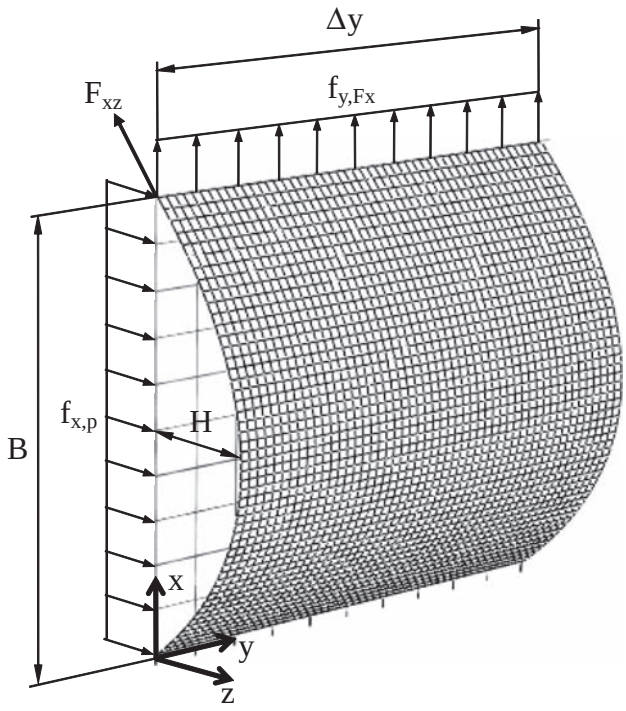

Fig. 5. Buckled polymer film segment for tensile stress calculation.

rupture of the polymer film. Thus, tensile stress within the PEEK film should not exceed 25 MPa and 2% elongation after 1000 h test duration to avoid mechanical breakdown.

3. Tensile stress calculation

Considering the heat exchanger and spacer geometry (Fig. 12), the actual mechanical load within the polymer film during operation has to be estimated for several reasons: (a) future selection of other suitable film materials for the heat transfer surface and (b) adaption of the spacer geometry for mechanical stabilisation of the polymer film. Therefore the tensile stress inside the polymer film was theoretically determined by calculations based on the tensile stress model described below.

3.1. Tensile stress model

A rope which is exposed to a uniform line load takes the form of a parabolic funicular curve (Eq. (2)), if self-weight is neglected and the rope is not affected by other forces [11]. This two dimensional model of a rope was expanded to a simplified three dimensional model, which is able to describe a buckled polymer film (Fig. 5). Like a rope, also a polymer film can only transmit tensile forces tangential to the film layer. No bending moments or shear forces can be applied to the film. A uniform line load turns to a (uniform) pressure in the three dimensional case. It is assumed that the edges of the film segment in parallel to the y-axis are non-relocatable. Amongst others, the distance B between these two edges is one parameter that determines the mechanical load into the polymer film. It corresponds to the (vertical) distance between the horizontal rods of the spacer grid (Fig. 12(a)). The film edges in parallel to the x-axis are assumed to be loose, because the polymer film is not in contact to the spacer's vertical rods (Fig. 12). The film buckling due to the fixation at the heat transfer surface's borders is neglected. This assumption simplifies the problem and is sufficient for the approximate determination of the maximum tensile stress and parameter variations with the used spacer geometry. In this case, film shape, as well as mechanical stress, is constant with respect to the y-coordinate (Eq. (4)). Thus, the shape of the polymer film according to Fig. 5 can be described by the following equation:

$$z = -4 \cdot \frac{H}{B} \cdot \left(\frac{x^2}{B} - x \right). \tag{2}$$

The first partial derivatives of Eq. (2) with respect to x and y are as follows:

$$\frac{\partial z}{\partial x} = -4 \cdot \frac{H}{B} \cdot \left(2\frac{x}{B} - 1 \right), \tag{3}$$

$$\frac{\partial z}{\partial y} = 0. \tag{4}$$

The pressure applied to the film is transformed to a uniform line load with respect to the x-direction:

$$f_{x,p} = p \cdot \Delta y. \tag{5}$$

Consequentially the force in parallel to the x-axis of the polymer film is calculated by Eq. (6), similar to a funicular curve's horizontal force [11]:

$$F_x = \frac{f_{x,p} \cdot B^2}{8 \cdot H}. \tag{6}$$

The force F_x is constant with respect to y. Therefore it can be written as a uniform line load:

$$f_{y,F_x} = \frac{F_x}{\Delta y} = \frac{p \cdot B^2}{8 \cdot H}. \tag{7}$$

F_{xz} represents the resulting force inside the polymer film layer. F_{xz} can be split into the two components F_x and F_z. The component F_x was already defined in Eq. (6). The component F_z is calculated by Eq. (8), with the first derivative with respect to x of the film shape function z (Eq. (2)):

$$F_z = \frac{\partial z}{\partial x} \cdot F_x. \tag{8}$$

Hence, the forces F_x and F_z can be described with Eqs. (9) and (10)

$$F_x = f_{y,F_x} \cdot \Delta y, \tag{9}$$

$$F_z = \left(\frac{\partial z}{\partial x}\right) f_{y,F_x} \cdot \Delta y. \tag{10}$$

Eq. (11) estimates the absolute value of the resulting force F_{xz} inside the film layer

$$F_{xz} = \sqrt{(F_x)^2 + (F_z)^2}. \tag{11}$$

Insertion of equations (9) and (10) into Eq. (11) leads to:

$$F_{xz} = \sqrt{\left(f_{y,F_x} \cdot \Delta y\right)^2 + \left(\left(\frac{\partial z}{\partial x}\right) \cdot f_{y,F_x} \cdot \Delta y\right)^2}. \tag{12}$$

The tensile stress is defined as follows:

$$\sigma = \frac{F}{A}. \tag{13}$$

The tensile stress is given by the ratio of the resulting force F_{xz} and the cross-sectional area, where L_0 is the original film thickness. With reference to tensile tests, the cross sectional area is based on the primarily cross-sectional area without taking the decrease of the cross-sectional area due to elongation into account:

$$\sigma_{xz} = \frac{F_{xz}}{L_0 \cdot \Delta y}. \tag{14}$$

Eq. (15) is obtained by insertion of Eq. (12) into Eq. (14). It describes the tensile stress σ_{xz} in the direction of the film layer depending on the x-coordinate

$$\sigma_{xz} = \frac{\sqrt{\left(f_{y,F_x}\right)^2 + \left(\left(\frac{\partial z}{\partial x}\right) \cdot f_{y,F_x}\right)^2}}{L_0}. \tag{15}$$

The case of plane stress is assumed with no shear stresses ($\tau_{\text{all directions}} = 0$) and no tensile stress in the y-direction. Principal stress and stress tensor then equals the tensile stress σ_{xz}

$$\sigma_p = \begin{pmatrix} \sigma_{xz} & 0 \\ 0 & 0 \end{pmatrix}, \tag{16}$$

$$\sigma_p = \sigma_{xz}. \tag{17}$$

The normal stress hypothesis is applied [12]. The maximum value of the principal stress is used for comparison with the allowed tensile stress. The polymer film can withstand the mechanical load, if the following inequation is satisfied

$$\sigma_{xz,\max} \leq \sigma_{\text{allowed}}. \tag{18}$$

Two components contribute to the elongation of the polymer film. The elastic elongation by mechanical stress is given by the ratio of tensile stress and Young's modulus. The second component is the thermal elongation, which is dependent on the linear coefficient of thermal expansion and the temperature difference to the reference temperature

$$\varepsilon_{xz} = \left(\frac{\sigma_{xz}}{E} + \alpha \cdot \left(\vartheta_{\text{exp}} - \vartheta_{\text{ref}}\right)\right). \tag{19}$$

The average elongation of the polymer film is obtained by integration of Eq. (19) and division by B

$$\varepsilon_m = \frac{\int_0^B \varepsilon_{xz}\, \mathrm{d}x}{B}. \tag{20}$$

The actual length b of the buckled polymer film with respect to x is then calculated using the average elongation.

$$b = B \cdot (1 + \varepsilon_m). \tag{21}$$

To get the resulting buckling height of the polymer film, Eq. (22) has to be solved. The information about the buckling height H is hidden into the function z (Eq. (2)). An analytical solution of Eq. (22) is described in [11].

$$b = \int_0^B \sqrt{1 + \left(\frac{\partial z}{\partial x}\right)^2}\, \mathrm{d}x. \tag{22}$$

It is mentioned for the sake of completeness, that the film thickness depends on the position in the x–y-plane. The film thickness can be calculated as a function of Poisson's ratio and elongation or average elongation, respectively.

$$L = L_0 \cdot (1 - \nu \cdot \varepsilon_{xz}), \tag{23}$$

$$L_m = L_0 \cdot (1 - \nu \cdot \varepsilon_m). \tag{24}$$

Combining equations (2), (5), (6), (7), (15), (19), (20), (21), and (22) yields a set of coupled nonlinear equations. The software Mathcad 2000 was used to solve these equations numerically and to obtain results for maximum tensile stress, elongation and buckling height of the polymer film.

3.2. Reference case for mechanical calculations

The parameters for the calculations were chosen with respect to the polymer film material (PEEK) and the expected operating conditions and geometries of the pilot plant (Table 3).

Table 3
Reference case parameters for tensile stress calculations

Film thickness L [m]	25×10^{-6}
Young's modulus E [Pa]	2000×10^{6}
Linear coefficient of thermal expansion α [K^{-1}]	47×10^{-6}
Reference temperature ϑ_{ref} for α [°C]	25
Mean operating temperature ϑ_{exp} [°C]	70
Pressure difference $\triangle p$ [Pa]	5000
(Vertical) distance between the spacer's horizontal rods B [m]	0.03

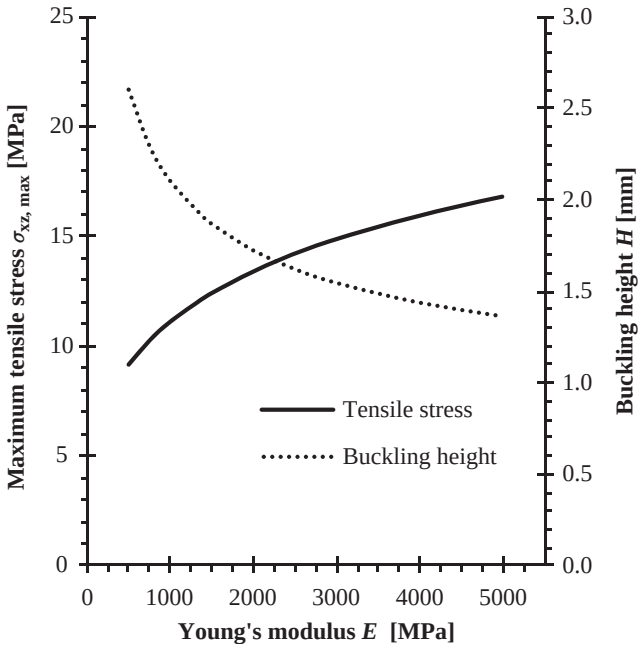

Fig. 6. Calculated tensile stress and buckling height of the polymer film.

3.3. Tensile stress modelling results

Several mechanical calculations on the basis of the model described in Section 3.1 were performed. Parameter variations are based on the reference case shown in Table 3, in order to estimate the influence of spacer and film geometries and mechanical properties of the polymer itself, on the polymer film's mechanical load. The results are shown in the following figures. As already mentioned above, it is important that the allowed tensile stress within the film should not exceed 25 MPa for reliable operation.

Fig. 6 shows the relation between the maximum tensile stress inside the film and the buckling height for different values of Young's modulus. It can be seen that a high Young's modulus implicates also a high tensile stress within the polymer film. This can be explained by the low elongation which is attended by a high Young's modulus. The low elongation leads to a small buckling height. Eq. (6) shows that the force F_x, and therefore the tensile stress, is increasing with decreasing buckling height. A small Young's modulus causes a lower tensile stress within the film due to further elongation. But it has to be taken into account that most polymers showing a small Young's modulus also have a smaller allowed tensile stress. Furthermore, the advanced elongation of materials with a small Young's modulus leads also to a decrease of the film cross-sectional area.

In order to vary the tensile stress of the polymer film, the film thickness can be altered (Fig. 7). A thin

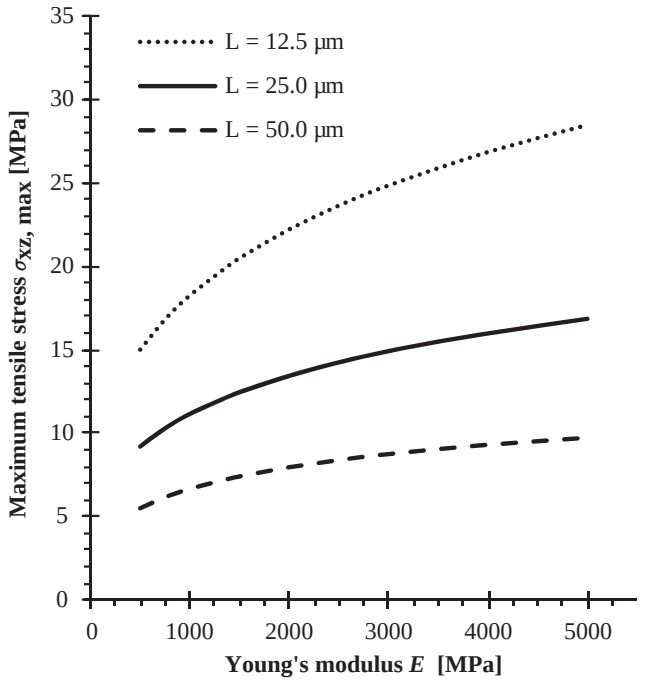

Fig. 7. Calculated maximum tensile stress within the polymer film for different film thickness.

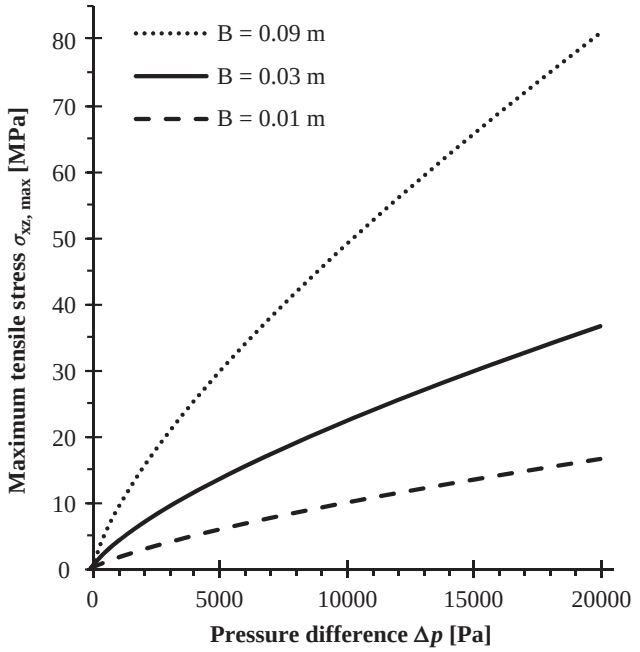

Fig. 8. Calculated tensile stress as a function of the spacer's horizontal rod distance and the pressure difference.

film induces a lower thermal resistance, which enhances the heat transfer in turn. The tensile stress of a 12.5 µm thick film approaches the above defined value of 25 MPa for the allowed tensile stress at a Young's modulus of about 3000 MPa. Obviously tensile stress is smaller in a thick polymer film. Unfortunately the thermal resistance is increasing at the same time. Therefore a 25 µm thick PEEK film seems to be the best compromise between mechanical strength and thermal resistance.

Another possibility to affect the tensile stress in the polymer film is to change the (vertical) distance between the horizontal rods of the wire mesh grid. It is shown in Fig. 8 that the tensile stress decreases with decreasing distance B. But the smaller the mesh size, the more of the heat transfer area is occupied by the spacers and is not directly available for heat transfer. It is reported that the spacer geometry has also an influence on the turbulence and consecutively on the convective heat transfer coefficient of the falling film [14,15]. If the pressure difference does not exceed 10000 Pa permanently, a distance between the horizontal rods of the wire mesh grid of 0.03 m should be sufficient for mechanical stabilisation of a 25 µm thick PEEK film.

Pre-buckling of the polymer film can also reduce the tensile stress of the film. This could be done by placing the polymer film in a loose manner on the spacers. According to Eq. (6) the force F_x and consecutively also the tensile stress will decrease with increasing (pre-) buckling height H.

As shown above, Young's modulus decreases when temperature increases between 30°C and 70°C (Table 2). Young's modulus was linearly interpolated between the experimental values for the calculations shown in Fig. 9 to obtain the maximum tensile stress for

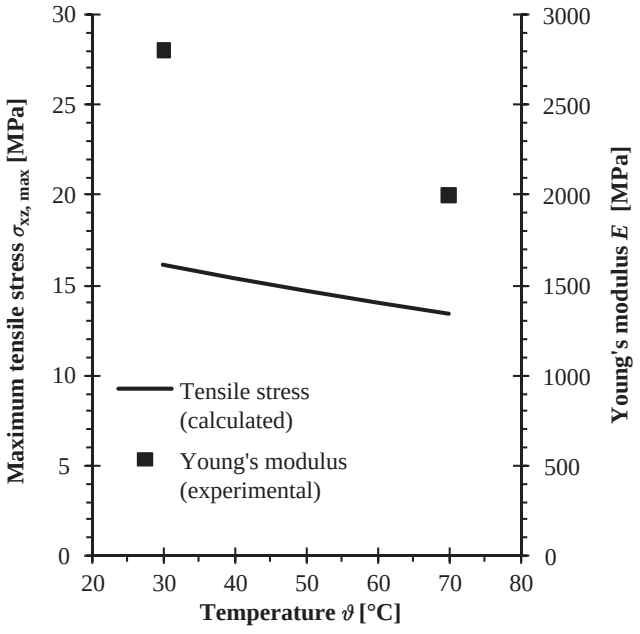

Fig. 9. Calculated tensile stress at different temperatures.

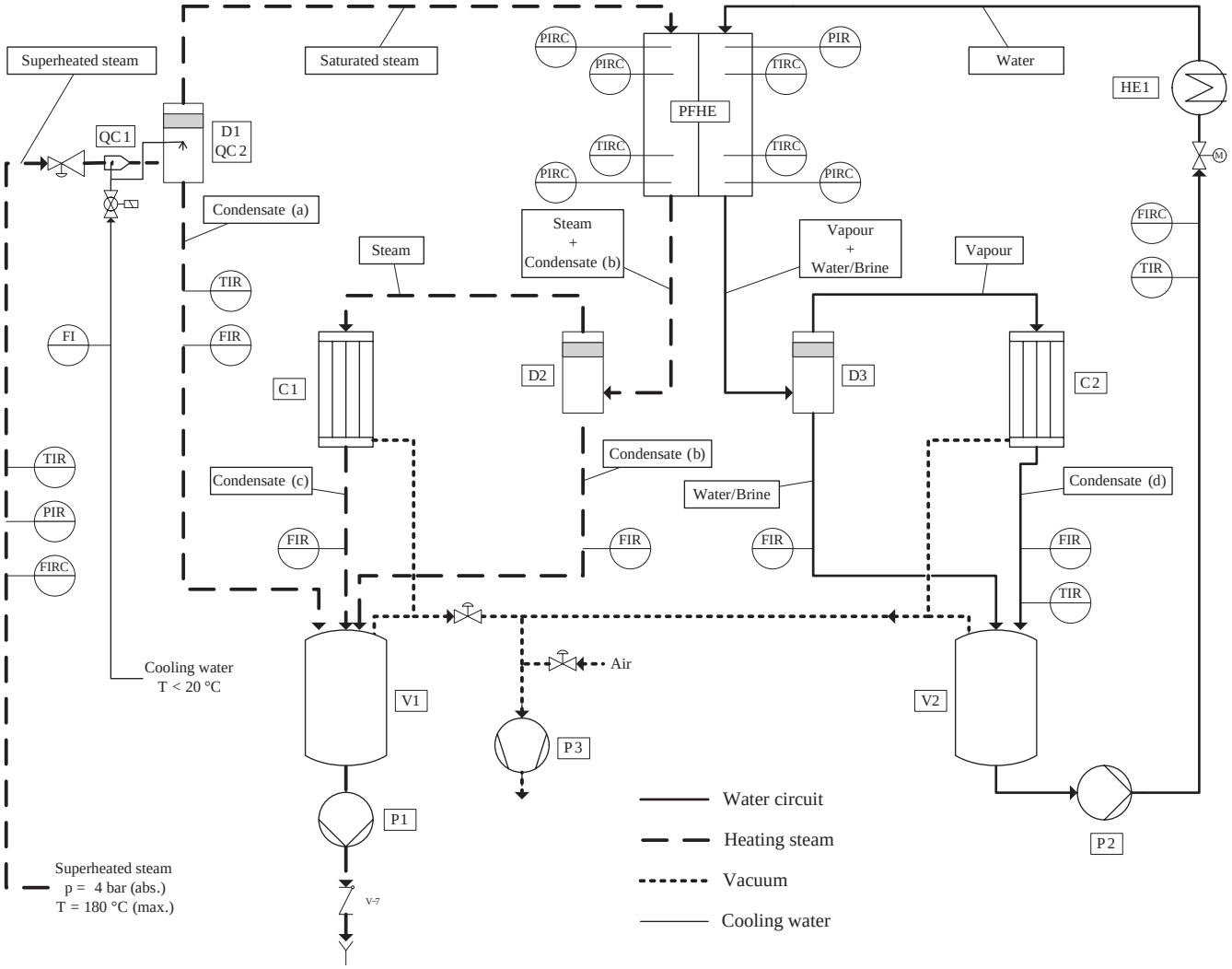

Fig. 10. Flow sheet of the pilot plant for heat transfer experiments. PFHE: Polymer film heat exchanger; C1, C2: Condensers; D1, D2, D3: Demisters; HE1: Heat exchanger; P1, P2, P3: Pumps; QC1, QC2: Quench coolers; V1, V2: Vessels.

temperatures between 30 and 70°C under typical MED operating conditions (Table 3). It was observed that 25 μm thick PEEK film can withstand the mechanical stress, because the allowed tensile stress of 25 MPa is not exceeded. It is interesting to notice that tensile stress within the film is decreasing with temperature. This effect is a result of the thermal expansion and the reduced Young's modulus at higher temperatures, which leads to an increased elongation and buckling height and therefore to a decrease of the force F_x and the mechanical load.

4. Polymer film heat exchanger

4.1. Pilot plant

A pilot plant was built to investigate the heat transfer performance of the developed polymer film plate heat exchanger. The process principle is according to a single effect falling film evaporator or a falling film heat exchanger, respectively. The overall mechanical construction of the plant allows operating temperatures up to 120°C and a pressure range from 0 Pa (abs.) to 110000 Pa (abs.). The process design was carried out to meet an operating point at 70°C and 31000 Pa with regard to typical operating conditions of MED-plants. Fig. 10 shows a simplified flow sheet of the pilot plant. Siphons, control lines, safety installations and additional valves are not displayed. Heating steam is always referred to as steam, whereas vapour depicts the evaporated water from the water circuit.

Superheated steam from a steam generator was expanded to the desired pressure and quenched (QC1, QC2) to the corresponding saturation temperature if necessary. The generated condensate (a) was

separated from the steam in a demister (D1) and directed into a condensate collection vessel (V1). The saturated steam served as heating steam. The heating steam entered the polymer film heat exchanger (PFHE) and was condensed on the heat transfer surface releasing latent heat. If the steam was not condensed entirely, a mixture of liquid condensate (b) and excess steam left the heating side of the apparatus. This mixture was separated in the demister D2. The excess steam was then condensed in condenser C1. The condensate (c) was guided to the condensate collection vessel V1 together with the condensate (b) from demister D2. The vessel was intermittently discharged by the gear pump P1.

The feed water to be heated or evaporated in the PFHE was stored in Vessel V2 and was pumped through the heat exchanger HE1 by the centrifugal pump P2, where it can be preheated to the desired PFHE entrance temperature or to the boiling point. The water entered the PFHE and was heated or evaporated while flowing over the polymer film heat transfer surface. The water and the vapour were separated in demister D3. The water was returned to vessel V2, whereas the vapour was condensed in condenser C2 before reaching vessel V2 again. A liquid ring vacuum pump (P3) with choke valves and leak air control was used for pressure adjustment.

The plant was equipped with adequate measurement instrumentations (Pt-100 thermometers, pressure sensors, ultrasonic-, magnetic-inductive and rotameter flow meters, etc.), to allow detailed heat and mass balancing. For process control and continuous data recording, sensors and valves were connected by FieldPoint modules to a PC equipped with LabVIEW 8.6.

4.2. Novel polymer film heat exchanger design

Fig. 11 shows an exploded view of the novel polymer film plate heat exchanger. It is constructed as a single effect falling film evaporator for the investigation of polymer film heat transfer surfaces under MED process conditions. It is not a one effect prototype for a multi effect distillation plant. The height and width of a heat transfer surface was 1 and 0.5 m, respectively. The prototype heat exchanger contained five polymer film heat transfer surfaces with a total area of 2.5 m^2 and a total liquid distribution length of 2.5 m. Water and heating steam were supplied co-currently from the top. Excess steam, condensate, heated water or brine and vapour left the heat exchanger at the bottom of the elements. The different elements were sealed by a flat gasket with the polymer film clamped in between. The gasket also serves as isolation to avoid heat flow between the evaporation and the condensation

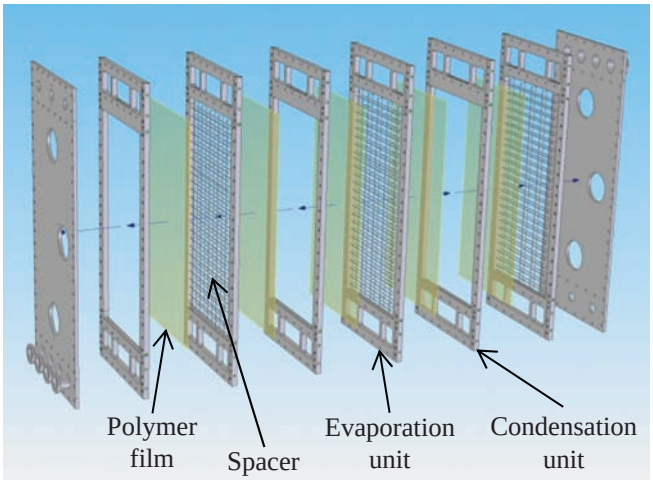

Fig. 11. Exploded assembly drawing of the novel polymer film heat exchanger.

elements due to the temperature difference. One element was 2.5 cm deep in order to minimise the pressure drop of steam/vapour flows. The two end plates were equipped with windows (circular holes shown in Fig. 11) to observe the water falling film and the condensing steam, respectively. Main parts of the prototype heat exchanger (frame, spacer) were made of stainless steel (1.4571 or 1.4301), because it is easy to purchase and the machining and the mechanical properties are well known. The heat exchanger and the pipes were isolated during operation, to minimise heat losses and to eliminate an influence of the surrounding temperature to the temperature profiles into the heat exchanger itself. 1.4571 and 1.4301 stainless steels are usually not used for heat exchanger parts in direct contact with hot seawater. Nevertheless, they should provide sufficient corrosion resistance for first fundamental experiments and proof of concept operation. To be competitive with present MED technologies, the use of polymers not only for the heat exchange surface, but also for other parts of the heat exchanger (housing, spacers, end plates etc.) is an interesting option. It was shown by Kafi et al. that polypropylene was successfully used as heat exchanger housing material for a MED-pilot plant [13].

4.2.1. Spacers

The pressure difference between the evaporation and the condensation side of the heat transfer surface, demands a design concept, which is able to take up the appearing mechanical load and to prevent the polymer film from rupture. Therefore, spacers were used to stabilise the polymer film (Fig. 12). The spacers consisted of a spot welded square mesh grid (stainless steel

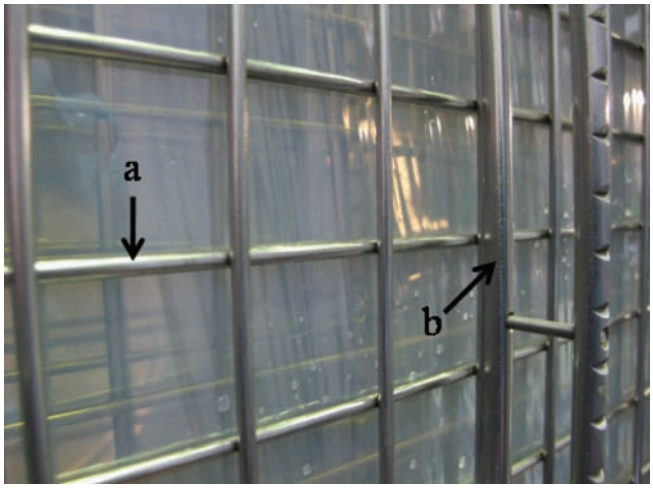

Fig. 12. Polymer film with spacers.

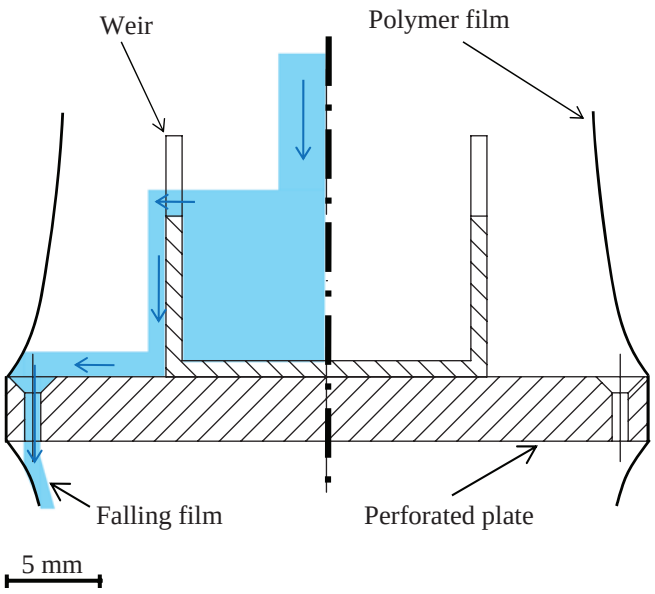

Fig. 13. Device for liquid distribution on polymer films with schematic liquid flow on the left hand side.

1.4301) with a mesh size of 3 cm and a wire diameter of 0.3 cm (Fig. 6(a)). The wire mesh is additionally stabilised by vertical rods behind (Fig. 6(b)). This arrangement allows the simple replacement of the grid. Only the horizontal rods of the grid are in direct contact with the polymer film. It is reported that such a grid also stabilises the falling film and therefore improves the wetting of the heat transfer surface [14]. A positive side effect is the enhancement of the heat transfer rate due to the spacers, because they act additionally as turbulence wires [15,16].

4.2.2. Liquid distribution

Uniform liquid distribution is of fundamental importance to establish a stable liquid layer on the polymer film surface. Therefore the water was predistributed by a serrated overflow weir at the top of the heat exchanger element. The liquid distribution to the polymer film itself was performed by a perforated polymethylmethacrylate (PMMA) plate (Fig. 13).

4.3. Heat transfer

Energy balances were used to calculate the mean overall heat transfer coefficient of the prototype heat exchanger at different operating conditions. On the heating side (steam, S), condensation (Eq. (25)) and probably condensate (C) cooling (Eq. (26)) is taking place. Saturated steam was assumed at the inlet. On the heated side (water circuit, W), heating of the flowing water (Eq. (27)) or evaporation (Eq. (28)) was considered. The pressure drops on both sides were neglected:

$$\dot{Q}_{S,C} = -\Delta h_S \cdot \dot{M}_{S,C}, \tag{25}$$

$$\dot{Q}_{S,C,c} = -\dot{M}_{S,C} \cdot c_{p,S,C} \cdot \left(\vartheta_{S,in} - \vartheta_{S,C,out}\right), \tag{26}$$

$$\dot{Q}_{W,L} = \dot{M}_{W,L} \cdot c_{p,W,L} \cdot \left(\vartheta_{W,L,out} - \vartheta_{W,L,in}\right), \tag{27}$$

$$\dot{Q}_{W,V} = \Delta h_W \cdot \dot{M}_{W,V}. \tag{28}$$

Also heat loss has to be considered. Therefore, further calculations were based on the heat uptake of the water circuit. The incomplete wetting of the polymer film surface can optionally be reflected by introduction of a wetting factor ω describing the surface wetting degree. The heat flow due to condensate cooling can only be neglected, if the amount of heat is very small (<1%), compared to the released latent heat of evaporation during condensation. For the case of condensation and heating of the water without evaporation, the mean overall heat transfer coefficient follows from Eq. (29) and Eq. (30), respectively

$$U_m = \frac{\dot{Q}_{W,L}}{A \cdot \Delta\vartheta_{m,log}}, \tag{29}$$

$$U_{m,\omega} = \frac{\dot{Q}_{W,L}}{A \cdot \omega \cdot \Delta\vartheta_{m,log}}. \tag{30}$$

If the feed water was evaporated or pre-heated with consecutive evaporation and condensate cooling can be neglected, Eqs. (31) and (32) have been used for estimation of the mean overall heat transfer coefficient:

$$U_{\mathrm{m}} = \frac{\dot{Q}_{\mathrm{W,L}}}{A \cdot \Delta\vartheta_{\mathrm{m,log}}} + \frac{\dot{Q}_{\mathrm{W,V}}}{A \cdot \Delta\vartheta_{\mathrm{m}}}, \tag{31}$$

$$U_{\mathrm{m},\omega} = \frac{\dot{Q}_{\mathrm{W,L}}}{A \cdot \omega \cdot \Delta\vartheta_{\mathrm{m,log}}} + \frac{\dot{Q}_{\mathrm{W,V}}}{A \cdot \omega \cdot \Delta\vartheta_{\mathrm{m}}}. \tag{32}$$

The mean logarithmic temperature difference in the case of condensing steam and (pre-) heating of the falling film is given by the following equation

$$\Delta\vartheta_{\mathrm{m,log}} = \frac{\left(\vartheta_{\mathrm{S}} - \vartheta_{\mathrm{W,out}}\right) - \left(\vartheta_{\mathrm{S}} - \vartheta_{\mathrm{W,in}}\right)}{\ln\left(\dfrac{\vartheta_{\mathrm{S}} - \vartheta_{\mathrm{W,out}}}{\vartheta_{\mathrm{S}} - \vartheta_{\mathrm{W,in}}}\right)}. \tag{33}$$

If the conditions correspond to the saturation state on both sides, without condensate cooling or water heating, the mean logarithmic temperature difference has to be replaced by a simple mean temperature difference (Eq. (34)).

$$\Delta\vartheta_{\mathrm{m}} = \left(\vartheta_{\mathrm{S}} - \vartheta_{\mathrm{W,out}}\right). \tag{34}$$

4.3.1. Wetting behaviour of the polymer film

Like most other polymers, PEEK exhibits hydrophobic surface characteristics, too. This is reflected in a high contact angle between water and PEEK in the system PEEK (s), water (l), air (g). The contact angles described in literature ranging from 50° to 85° for untreated PEEK, depending on the measuring method [7,17]. The wettability of polymers can be enhanced by different methods like formation of hydrophilic groups on the surface, corona and gas plasma discharge methods [18] or roughening of the surface [19]. Untreated PEEK film was used for heat transfer experiments. The untreated polymer film's falling film wetting degree in the system PEEK (s), water (l), air (g) was determined photooptically at different liquid loads to estimate the fraction of the wetted heat transfer area. Therefore additional experiments with an accessory apparatus were carried out. The apparatus had the same spacer and liquid distribution device than the pilot plant heat exchanger (see 4.2). It was made of Polymethylmethacrylate (PMMA) to observe the falling film wetting on the whole PEEK-film surface. The experiments were performed at increasing and decreasing liquid loads, respectively, to take advancing and receding liquid interfaces into account. The resulting mean value of the wetting degree and the formula for the corresponding regression line is shown in Fig. 14 and Eq. (35), respectively. It is self-evident that Eq. (35) should only be used for interpolation, but not for extrapolation of the wetting degree. The wetting

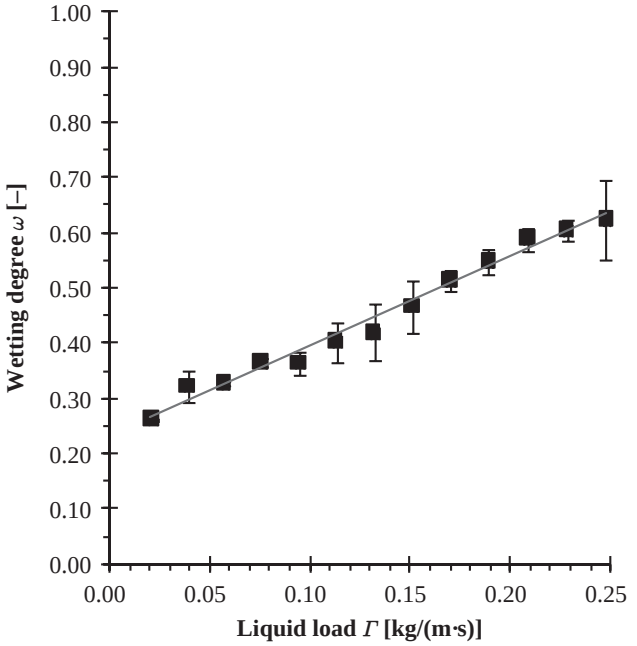

Fig. 14. Wetting behaviour of untreated PEEK film.

experiments were performed with distilled water at room temperature on air. The wetting behaviour of an evaporating seawater falling film under vacuum may be considerably different. Hence, the results shown in Fig. 14 and Eq. (35) are only a rough estimation for the wetting degree under operating conditions.

$$\omega = 1.609 \cdot \Gamma + 0.233. \tag{35}$$

4.3.2. Experimental overall heat transfer coefficients

To determine the thermal performance of the novel polymer film heat exchanger, heat fluxes were measured and the mean overall heat transfer coefficient was calculated according to Eqs. (25) to (35). The operating conditions of the heat exchanger and the experimental results for the mean overall heat transfer coefficient are listed in Table 4. Drinking water was used as test liquid in order to avoid boiling point elevation and to be able to use magnetic-inductive flow meters for proper energy balancing. Partial wetting of the heat transfer surface was not taken into account when calculating the mean overall heat transfer coefficients U_{m}. This is reflected by referring to the total, instead of the wetted heat transfer surface. Nevertheless the observed coefficients reach values between 1300 and 1600 $\mathrm{W/m^2 \cdot K}$ when condensation and evaporation takes place. Kafi et al. used a plate evaporator heated with hot water and observed heat transfer coefficients of about 900 to 1200 $\mathrm{W/(m^2 \cdot K)}$, depending on the applied liquid load [14]. The difference of the

Table 4
Operating conditions and experimental mean overall heat transfer coefficients

Experiment No.	1	2	3	4
Inlet temperature heating steam $\vartheta_{S,in}$ [°C]	101	100	72	73
Pressure heating steam p_S [kPa]	105	102	34	36
Inlet temperature water $\vartheta_{W,in}$ [°C]	51	85	66	67
Pressure water p_W [kPa]	99	98	30	31
Evaporation	No	No	Yes	Yes
Liquid load water Γ [kg/(m·s)]	0.036	0.173	0.115	0.145
Mass flow of the evaporated water [kg/s]	–	–	0.0041	0.0056
Mean overall heat transfer coefficient U_m [W/m^2·K]	314 ± 17	446 ± 31	1341 ± 210	1570 ± 181
Approximated wetting degree ω [–]	0.29 ± 0.03	0.51 ± 0.03	0.42 ± 0.03	0.47 ± 0.03
Modified mean overall heat transfer coefficient $U_{m,\omega}$ [W/m^2·K]	1075 ± 131	873 ± 81	3207 ± 558	3375 ± 452

overall heat transfer coefficients is most likely based on the better convective heat transfer coefficient due to condensation compared to one phase forced convection. The observed experimental heat transfer coefficients are thus in a technically common range. In contrast, the heat transfer coefficients for operation with only heating of the falling film were very low (<500 W/(m^2·K)) and did not reach a competitive magnitude. This observation is most likely based on an enhancement of the convective heat transfer coefficient due to evaporation of the falling film. The heat transfer coefficient was increasing with liquid load, owing to the higher turbulence of the falling film.

As shown above, it can be supposed that the heat transfer surface was not wetted completely, because of the use of untreated PEEK films. Then, the area actually used for heat transfer was computed by multiplying total heat transfer area and wetting degree. The wetting degree can be approximated using Eq. (35). The obtained modified mean overall heat transfer coefficients $U_{m,\omega}$ were significantly larger than the original ones. They took values of about 3200 to 3400 W/(m^2·K) for condensation and evaporation. Kafi et al. [13] reported overall heat transfer coefficients in the second effect of a MED pilot plant of about 2500 to 3700 W/m^2·K for condensation and seawater evaporation. But the values for the modified mean overall heat transfer coefficients $U_{m,\omega}$ have to be taken with care. It has to be kept in mind that they are referred to a theoretically estimated wetted heat transfer surface area, which is smaller than the total heat transfer surface area. They do not really represent measured values and they are probably overestimated because of the different wetting behaviour of the polymer film at operating conditions (high temperatures, evaporation, vacuum) compared to the conditions where Eq. (35) was derived (ambient pressure and temperature, no evaporation). To make this approximation dispensable, further research should focus on the maximisation of the wetting degree in the range of technically relevant liquid loads. Polymer film pretreatment, modification of the liquid distribution device and the spacer geometry are the major parameters for the improvement of the heat transfer efficiency. Obviously, the heat transfer performance is best when the available heat transfer surface is totally wetted.

5. Conclusions

The mechanical behaviour of 25 μm thick PEEK film was determined in water at different temperatures. The allowed tensile stress for permanent application of the PEEK film under hot and wet conditions should be reduced far below the allowed tensile stress according to ISO 527. Based on these experimental results, calculations of the tensile stress within the polymer film showed, that the selected PEEK film in combination with the spacer geometry is able to withstand the expected temperature and pressure differences. Heat transfer experiments displayed realistic results for the mean overall heat transfer coefficient and even better results when they were corrected by the wetting degree of the heat transfer surface. The complete wetting of the heat transfer surface is essential for a cost-effective operation of falling film evaporation plants. More detailed research on this aspect is of main interest for further investigations.

Acknowledgement

The project (240 ZN) was funded by the Federal Ministry of Economics and Technology (BMWi) through the German Federation of Industrial Research Associations (AiF).

Symbols

A Area, m^2
b Polymer film length with respect to x

B	Distance between the horizontal rods of the spacer grid / Film segment length with respect to x, m
c_P	Heat capacity at constant pressure, J/(kg·K)
E	Young's modulus, Pa, MPa
f	Uniform line load, N/m
F	Force, N
h	Convective heat transfer coefficient, W/(m^2·K)
H	Buckling height, m
k	Thermal conductivity, W/(m·K)
L	Thickness heat transfer surface, film thickness, m, μm
$\dot{M}$	Mass flow rate, kg/s
p	Pressure, Pa, kPa
$\dot{Q}$	Heat transfer rate, W
R	Thermal resistance, K/W
U	Overall heat transfer coefficient, W/(m^2·K)
x	Cartesian coordinate, m
y	Cartesian coordinate, m
z	Cartesian coordinate, m

Greek letters

α	Linear coefficient of thermal expansion, K^{-1}
$\triangle y$	Length difference with respect to the y coordinate
$\triangle h$	Latent heat of vaporisation, J/kg
$\triangle p$	Pressure difference, Pa
$\triangle \vartheta$	Temperature difference, °C
ε	Elongation, –
ϑ	Temperature, °C
Γ	Liquid load, kg/(m·s)
ν	Poisson's ratio, –
σ	Tensile stress, Pa, MPa
τ	Shear stress, Pa
ω	Wetting degree (m^2_{wet}/m^2_{total}), –

Indices

0	Primary dimension
allowed	Maximum allowed, allowable
c	Cold, cooling
C	Condensate
cd	Conduction, conductive
exp	Experimental
F	Force
in	Inlet
h	Hot
L	Liquid
log	Logarithmic
m	Mean, average
max	Maximum
out	Outlet
p	Pressure
ref	Reference
S	Steam, heating steam, heating side
tot	Total
V	Vapour (water circuit, heated side)
W	Water, water circuit, heated side
wall	Wall, heat transfer surface
x	Cartesian coordinate
xz	Film plane with respect to x and z coordinates
y	Cartesian coordinate
yz	Film plane with respect to y and z coordinates
z	Cartesian coordinate
ω	Wetted, referred to the wetted area

References

[1] L. Ramm-Schmidt, Chem. Eng., 783 (2006) 39–41.
[2] L. Zaheed and R.J.J. Jachuck, Appl. Thermal Eng., 24 (2004) 2323–2358.
[3] G. Hetsroni and A. Mosyak, Chem. Eng. Process., 33 (1994) 91–100.
[4] T.B. Scheffler, A.J. Leao, Desalination, 222 (2008) 707–721.
[5] H. Domininghaus, Die Kunststoffe und ihre Eigenschaften, VDI-Verlag GmbH, Düsseldorf, 1992.
[6] M. Al-Shammiri and M. Safar, Desalination, 126 (1999) 45–59.
[7] Manufacturer Information, Victrex plc.
[8] J.R. Burns and R.J.J. Jachuck, Appl. Thermal Eng., 21 (2001) 495–510.
[9] O. Schwarz, Kunststoffkunde, Vogel Verlag und Druck KG, Würzburg, 1990.
[10] C. Wegst and M. Wegst, Stahlschlüssel, Verlag Stahlschlüssel Wegst GmbH, Marbach, 2007.
[11] D. Gross, W. Hauger and P. Wriggers, Technische Mechanik Band 4: Hydromechanik, Elemente der Höheren Mechanik, Numerische Methoden, Springer-Verlag, Berlin Heidelberg, 2007.
[12] D. Gross, W. Hauger, W. Schnell and J. Schröder, Technische Mechanik Band 2: Elastostatik, Springer-Verlag, Berlin Heidelberg, 2005.
[13] F. Kafi, V. Renaudin, D. Alonso, J.M. Hornut and M. Weber, Desalination, 182 (2005) 175–186.
[14] F. Kafi, V. Renaudin, D. Alonso and J.M. Hornut, Desalination, 166 (2004) 53–62.
[15] H. Raach and J. Mitrovic, Desalination, 183 (2005) 307–316.
[16] W.M. Salvagnini and M.E.S. Taqueda, Ind. Eng. Chem. Res., 43 (2004) 6832–6835.
[17] N.L. Franchina and T.J. McCarthy, Macromolecules, 24 (1991) 3045–3049.
[18] I. Noda, Chem. Ind., 20 (1991) 749–752.
[19] S. Palzer, C. Hiebl, K. Sommer and H. Lechner, Chem. Ing. Tech., 73 (2001) 1032–1038.